Trans Indian Inst Met (2017) 70(1):115–124
DOI 10.1007/s12666-016-0866-z

TECHNICAL PAPER

Microstructure and Mechanical Behavior of X90 Bend Using Local Induction Bending

Bin Wang[1] · Liang Wang[1] · Yong Jiang[2] · Ming Xu[1] · Bo-bo Lei[1] · Yiwen Hu[1] · Deng Wu[1] · Zhengyang Luo[1] · Liyan Liu[1]

Received: 27 August 2015 / Accepted: 19 February 2016 / Published online: 25 April 2016

Abstract The microstructure and mechanical properties was studied for API (American Petroleum Institute) X90 pipeline steel bend, which was formed by local induction heat. It was found that X90 pipeline steel parent microstructure consisted of quasi-polygonal ferrite, granular bainite and a small amount of M/A constituents, which provided a good mechanical property. The yield strength, tensile strength, and yield ratio was 786, 876 MPa, 0.90, respectively. After local induction bending, strain-induced phase transition behavior occurred within the deformation zone. The neutral axis position was almost free from force, for quenching-tempering microstructure with small grains. Compared to the parent pipe, the strength decreased after local induction bending. At −10 °C, the Charpy impact absorbed energy was higher, which showed good toughness. In addition, the ductile–brittle transition temperature was studied during −20 ∼ −40 °C in outer arc side. At −60 °C, the impact absorbed energy was 27 J, which was not suitable for a pipeline.

Keywords X90 steel · Local induction bending · Microstructure · Mechanical properties · Toughness

✉ Liang Wang
lwang1314@aliyun.com

[1] School of Materials Science and Engineering, Southwest Petroleum University, Chengdu 610500, China

[2] Atlantic Welding Materials Co., Ltd, Zi Gong 643000, China

1 Introduction

As consumption of energy is increasing worldwide, the demand for development of economic tool for oil and gas pipeline construction has become high. Pipeline development from X60, X70, X80 to X90, X100 and other higher-level development, exhibit a high-level yield strength [1]. High strength and toughness help reducing wall thickness, improving the ability to stop cracks, and lower the construction costs [2–4]. So the development of oil and gas transmission and metallurgical industries have received widespread attention.

In the oil and gas pipeline construction, according to the topography changes, ground movement or buffering external forces exerted on the pipe, requires a lot of bends. Induction heating is an advanced process that is widely used to bend pipes with small bending radius and large diameter. It is efficient, low-cost and provide products with good material properties [5–11].

The microstructure development and mechanical properties of these bends are strongly influenced by the parameters of heat treatments conditions and the mother pipe chemical compositions. Although the quenching and tempering is a very effective technique to get the optimum balance of strength and toughness [12, 13], the bends having large-diameter and thick-walls are difficult to get with uniform strength and toughness, especially for the high strength pipeline.

Many scholars have carried out researches, which have produced many successful outcomes and ensured the safety of construction projects. Zhong et al. [5] and Zutang et al. [10] used the computer simulation system combined with the theory of pipe-bending to to simulate the whole process of pipe bending using local induction heating with small bending radius. The results, such as the thinning and thickening ratio of pipe wall thickness, the ovality of the

cross-section of the pipe, the spring-back angle after unloading, the bending force and the reverse movement, can be obtained using this computer simulation system. Wang et al. [14] investigated the continuous cooling transformation (CCT) diagrams and the effects of heat treatments on microstructure and properties to design heavy walled thickness bends. Kathayat et al. [11] indicated that more aggressive peak temperature (Above Ac3) and cooling during induction bending can prevent significant deterioration in material properties. On the other hand, many studies have been performed to evaluate the effects of hot bending parameters on microstructure and mechanical properties of thick-walled pipe bends, and the relationship of microstructure and mechanical properties under hot induction bending [15–18].

In this work, X90 pipeline steel with large-diameter and thick-wall has been selected to investigate the microstructure and mechanical behavior after local induction bending. The local induction parameters has been determined by theoretical calculations and referring the local induction parameters of X80 pipeline steel [15, 18]. The effect of the local induction on microstructure and mechanical properties has been studied. According to the results, determination of the process parameters are practical. Furthermore, the relationship of microstructure and the strength-toughness for X90 bend have been investigated.

2 Material and Experimental Procedures

2.1 Experimental Material

The chemical composition of X90 pipeline steel are shown in Table 1. The experimental steel was manufactured into Φ1219 × 26.4 mm weld pipe by submerged arc welding. Its mechanical properties are summarized in Table 2, the yield strength, tensile strength, and yield ratio was 786, 876 MPa, 0.90, respectively which met the requirements of API 5L standard [1]. The X90 pipeline steel presented quasi-polygonal ferrite (QPF) with the presence of granular bainite (GB) and a small amount of martensite/austenite (M/A) constituents (see Fig. 1). From Fig. 1, it can be figured out that the ferrite and bainite have uniform distribution, together with M/A islands in the form of granular or elongated dispersions therein.

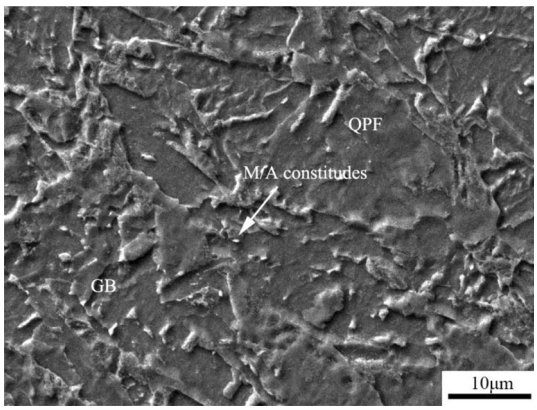

Fig. 1 SEM image of X90 pipeline steel (Nitial etching)

2.2 Local Induction Bending Process

The outline of pipe bending using local induction bending is shown in Fig. 2a. Firstly, medium-frequency induction heating was performed on the X90 mother pipe to Ac_3 temperature and thereby austenitizing the material. Then, the heating zone around a fixed center of rotation at a fixed pivot arm and pushing load for bending a fixed radius of curvature bend. To ensure the mechanical properties of the material after bending, heating and water cooling were needed simultaneously. During pipe bending, the wall of bending outside was thinned owing to tensile stress and the wall of the bending inside was thickened because of compression stress. In addition, the cross-section of bend pipe became oval, and the position of weld joint in the bending inside was 45 °C with the central axis as shown in Fig. 2b. After the pipe bend was formed, tempering treatment was essential to eliminate the residual stress, to achieve the purpose of quenching-tempering, which resulted in the excellent mechanical properties.

Table 1 Chemical composition of the used steel (wt%)

	C	Mn	P	S	Si	Nb	V	Ti	Cu	Cr	Mo	Ni	B	CEqcm
X90	0.065	1.82	0.012	0.003	0.281	0.044	0.018	0.013	0.148	0.022	0.426	0.375	0.0007	0.21

Table 2 Mechanical properties of the used steel

	Yield strength Rt0.5 (MPa)	Tensile strength Rm (MPa)	Elongation A50 mm (%)	Yield ratio Rt0.5/Rm	Average impact absorbed energy at 0 °C (J)
X90	786	876	17.5	0.90	213

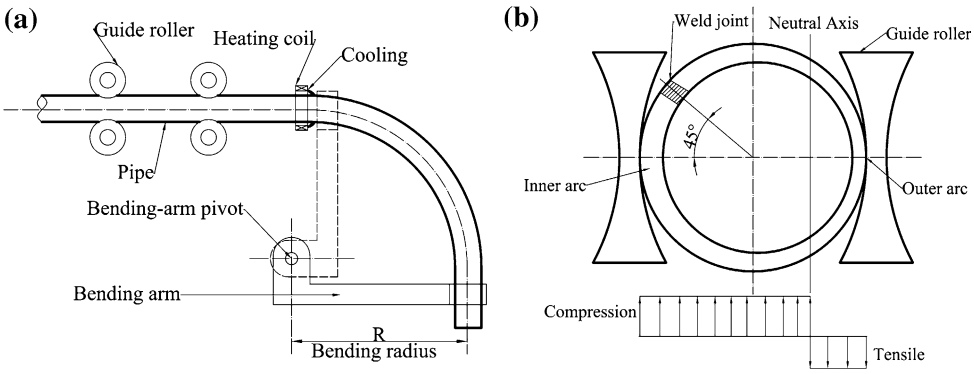

Fig. 2 Model of the hot pipe bending process using local induction heating: **a** outline of pipe bending; **b** position of neutral axis and weld joint

Table 3 Local induction bending parameters of X90 pipeline steel

Heating temperature (°C)	Push speed (mm/min)	Cooling water flow (m^3/h)	Bending angle (°)	Tempering temperature (°C)	Holding time (min)	Cooling
1000	25	44	7	560	70	Air Cooling

As the CEqcm of the experimental steel was 0.21, the Ac_3 temperature was 930 °C, calculated by Thermocalc software according to the chemical composition and mechanical properties of X90 pipeline steel. The corresponding local induction bending parameters for X90 were worked out by referring to the local induction bending process parameters for X80 pipeline steel [15, 18], such as the induction heating temperature, push speed, cooling water flow and tempering temperature, as summarized in Table 3.

2.3 Microstructural Observation and Mechanical Properties Tests

The microstructure specimens were machined from different positions of the X90 pipe, namely from the outer arc side, inner arc side, and from the central neutral position (Fig. 3). The specimens for microstructural studies were mechanically polished using standard metallographic procedures and etched with a 4 vol% nital solution and observed using a Leica DMIRM optical microscope (OM) and Zeiss Ultra 55 scanning electron microscope (SEM). The fractured surfaced of impact specimens was studied by an FEI Quanta 600 SEM.

Tensile specimens of dimensions 12.5 mm diameter and 50 mm gauge length and charpy v-notch impact specimens of dimensions $10 \times 10 \times 55$ mm^3 were machined from the X90 bend at different positions, namely from outer arc side, inner arc side and the neutral axis position, parallel to the longitudinal and transversal direction. The tensile tests were conducted at room temperature using a crosshead speed of 3 mm/min using a SHT 4605 testing machine. Charpy v-notch impact tests were performed at −10 °C, performed on the JB-500B impact tester consistent with

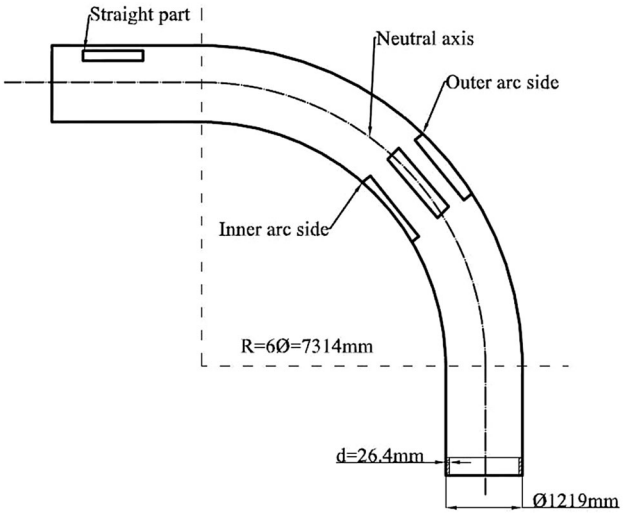

Fig. 3 Schematic illustration of different positions of X90 bend

ASTM E23 specification [19]. In order to study the ductile–brittle transition temperature of X90 bend pipe, the outer arc side was selected because this region was the weakest region of the bend pipe, and the important key part of bend. The specimens were cooled to −2 °C below the test temperature to take into consideration the rise in temperature during transfer of specimens to the impact tester. This temperature was tested by a digital thermometer.

3 Experimental Results and Analysis

3.1 Microstructure After Local Induction Bending

Optical and SEM micrographs of X90 bend pipe at different positions are presented in Fig. 4. The differences in

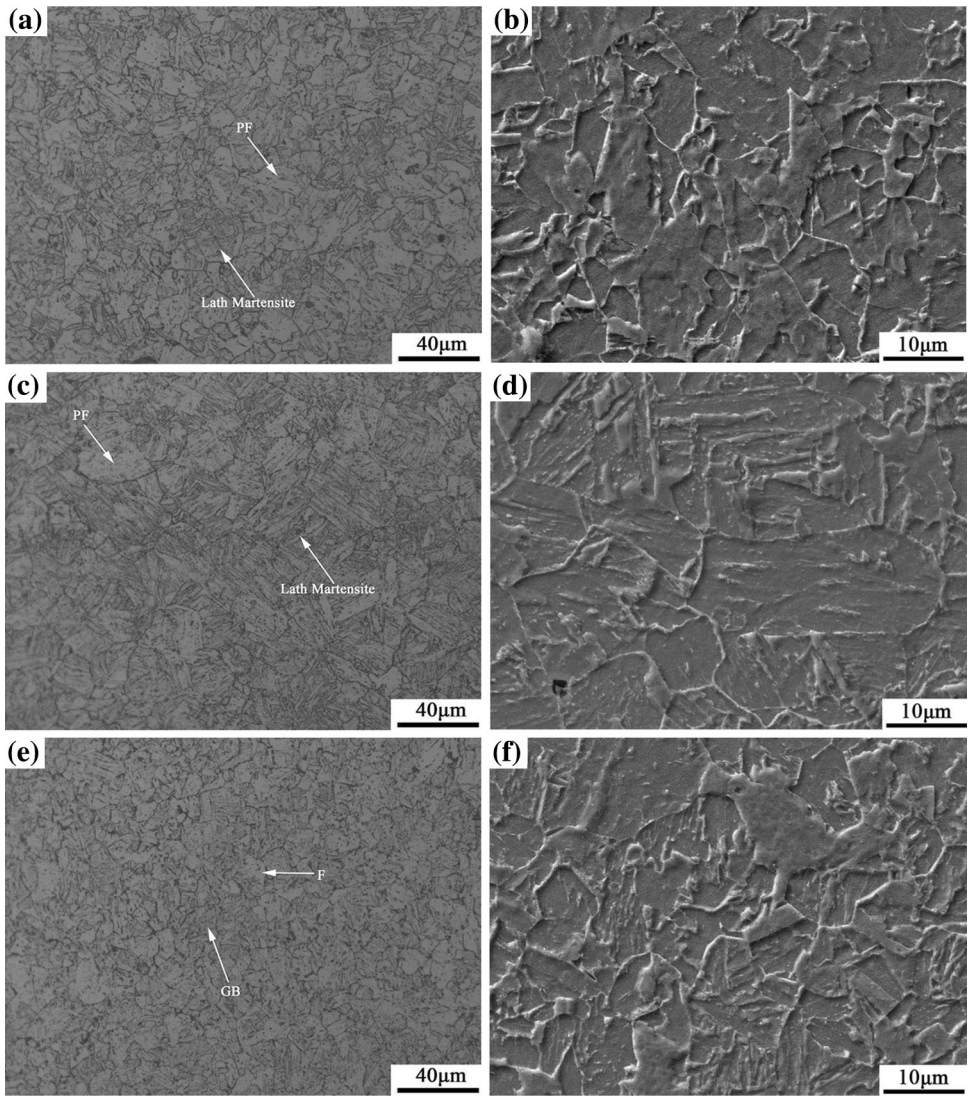

Fig. 4 OM and SEM micrographs of X90 bend at different positions: **a** OM of inner arc side; **b** SEM of inner arc side; **c** OM of outer arc side; **d** SEM of outer arc side; **e** OM of the neutral axis position; **f** SEM of the neutral axis position

the microstructure can be observed in terms of morphologies. At the outer (Fig. 4a, b) and inner arc side (Fig. 4c, d), the microstructure consists of polygonal ferrite and lath martensite, and the polygonal ferrite is nucleated at the prior austenite grain boundaries, while the martensite laths are nucleated intra granularly. Compared to polygonal ferrite, the martensite consists of more slender and interwoven ferrite laths or plates. At the neutral axis position (Fig. 4e, f), the microstructure consists of ferrite and granular bainite.

According to the stress of bending process, the inner arc side (a, b) and the outer arc side (c, d), respectively, are subjected to compression and tensile stress, where in a great amount of deformation occurs, resulting in microstructural differences at the position of the neutral axis (e, f) which is almost free from force. Compared to Fig. 1, the microstructure in the X90 bend pipe is different from that observed in the mother pipe, with the inner and the outer arc side consisting of polygonal ferrite and lath martensite, while granular bainites are hardly observed. Due to the characteristic in the process of local induction bending with quenching during deformation, as suggested by Beladi et al. [20], unlike the static transformation in conventionally thermomechanical processed austenite, which only provides a fixed number of nucleation sites, the ongoing deformation during dynamically strain-induced phase transformation (DSIT) can enable more nucleation sites in the interior of austenite grains, thus promoting extensive intra granular nucleation of martensite.

Fine polygonal ferrite is formed during bending, which is generated by dynamically strain-induced phase transformation [21]. When the temperature decreases to the initial martensitic transition temperature during quenching, the residual austenite is transformed into martensite, with the martensite laths almost parallel, long and thin. During the later part of the tempering process, a part of carbide is

Table 4 Tensile tests results of X90 pipe after local induction bending

Specimens	Yield strength Rt0.5 (MPa)	Tensile strength Rm (MPa)	Elongation A50 mm (%)	Yield ratio Rt0.5/Rm
Straight bend	710	821	20	0.86
Inner arc side longitudinal	706	802	24	0.88
Inner arc side transversal	703	789	24	0.89
Outer arc side longitudinal	750	848	21	0.88
Outer arc side transversal	703	796	20	0.88
The neutral axis	693	785	22	0.88

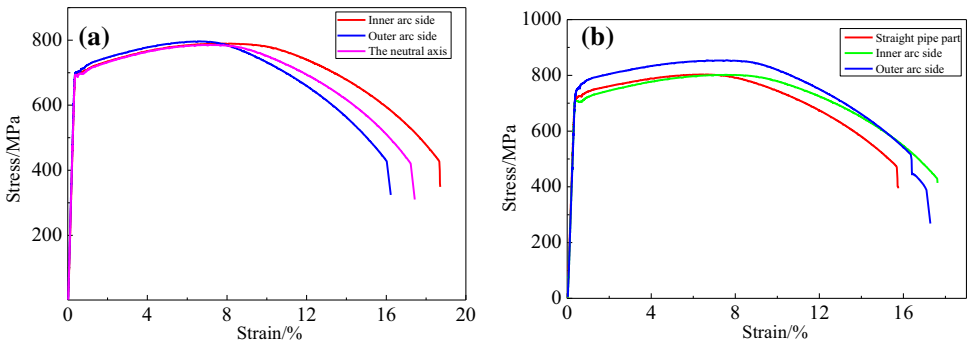

Fig. 5 The tensile stress–strain plots of X90 local induction bending: **a** Transversal; **b** longitudinal

precipitated on the matrix and lath martensite grain boundaries become blur. For the neutral axis position almost free from force [22], which is similar to quenching without deformation, the heat treatment is similar with the static transformation process.

3.2 Tensile Properties

Table 4 summarizes the tensile test data of X90 bend at different positions, namely at inner, outer arc side and at the neutral axis position (Fig. 1). For comparison, some specimens have also been taken from the unbend pipe. The tensile strain–stress plots are presented in Fig. 5. From Table 4, it is evident that after local induction bending, the yield strength of the X90 pipe at different positions are lower than that of the mother pipe by at least 20–30 MPa when compared with the strength of mother pipe as shown in Table 2. The yield strength, tensile strength, elongation and yield ratio for outer arc side parallel to longitudinal direction is 750, 848 MPa and 0.88, respectively, and percentage of elongation-to-fracture is 21 %. The yield strength, tensile strength, elongation and yield ratio for inner arc side parallel to longitudinal direction is 703, 796 MPa and 0.88, respectively, and percentage of elongation-to-fracture is 20 %. The reason why the strength in outer arc side is higher than what in inner arc side parallel to longitudinal direction is related to the stress during bending process. There is tensile stress state along the outer arc side, and the compressive stress along the inner arc side. Comparing the tensile stress–strain plots in Fig. 5, it is evident that yield platform appear both in the outer arc side and in the inner arc side after bending. It means that the grain size of the X90 parent pipe becomes large and the dislocation density decreases after quenching and tempering [23]. The work hardening and the process of dynamic softening are conducted simultaneously while heating and pushing. Since the deformation temperature is higher than the recrystallization temperature, hardening caused by deformation is quickly eliminated by the recrystallization softening process. Since the heating zone is not wide, and the advancing speed is slower, the quenching zone is reheated, the grain growth occurs and the dislocation density decreases after the temperature is increased, resulting in yield platform.

3.3 Charpy Impact Properties

The impact absorbed energy of X90 bend obtained at different positions and tested at −10 °C is presented in Table 5. The average impact absorbed energy at the straight pipe part, the neutral Axis, inner and outer arc side are 222 J, 220 J, 225 J, 153 J, respectively. While there is no difference in the average energy of the straight pipe part, the neutral Axis, inner arc side, the average energy of outer arc side by tensile stress is the lowest with a value of only 153 J.

Table 5 Low temperature impact absorbed energy in local bend

Samples	Impact absorbed energy (−10 °C) Kv_8 (10 × 10 × 55)							
	J				SA %			
	1	2	3	Avg.	1	2	3	Avg.
Straight pipe	210	235	225	223	70	80	80	77
Inner arc side of bend	220	225	230	225	90	90	90	90
Outer arc side of bend	150	175	135	153	40	60	40	47
Neutral axis	205	235	220	220	90	90	90	90

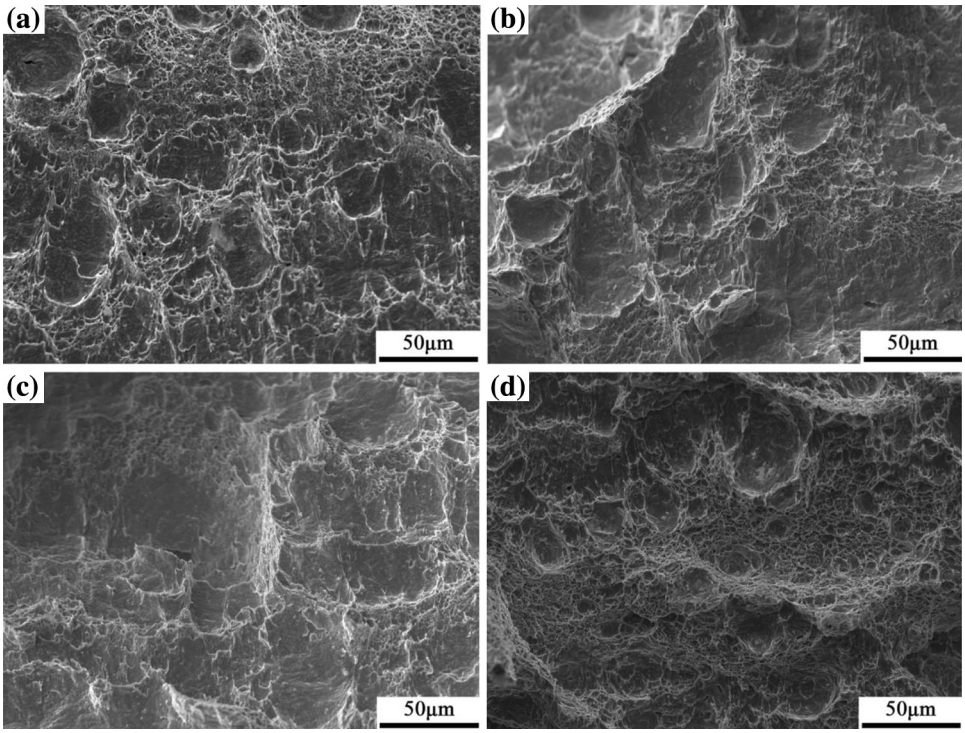

Fig. 6 Charpy impact fracture morphology at different parts of X90 bend at −10 °C **a** the straight pipe part; **b** inner arc side; **c** outer arc side; **d** the neutral axis

High magnification SEM fractographs of impact toughness tested at different positions are presented in Fig. 6. It can also be seen from the impact fracture morphology as shown in Fig. 6 that the dimples in outer arc side (Fig. 6c) are shallow, compared to the straight pipe part (Fig. 6a), inner arc side (Fig. 6b) and the neutral axis (Fig. 6d), which is resulted by tensile stress; in addition, there are large and small-sized dimples in the neutral axis (Fig. 6d) fiber fracture zones, which are deep, and prove good fracture toughness. Small-sized dimples are mainly from carbide particles precipitated in the matrix after tempering treatment. Low temperature impact properties of X90 local induction bending is closely related to the forces and microstructure. Although similar microstructures exist in inner and outer arc side, the former are pressed while the latter are pulled, resulting in different impact toughness.

Since the impact absorbed energy of X90 bend outer arc side is lower than the others, therefore, this area has been selected to plot ductile–brittle transition curve to study its ductile–brittle transition temperature. The impact absorbed energy of the outer arc side in X90 local bend at different temperatures is shown in Table 6 and the ductile–brittle transition curve is shown in Fig. 7. The impact tests data point out that the impact energy AKV of outer arc side in X90 bend decreases with the decrease of test temperature. It can be seen from Fig. 7 that the low temperature impact toughness is excellent, which is close to 231 J at 0 °C, and reaches 175 J at −20 °C. However, impact toughness decreases rapidly at −20 ∼ −40 °C, and reaches 64 J at −40 °C. Thus it can be inferred that the ductile–brittle transition temperature is −20 ∼ −40 °C, and the low temperature impact toughness is only 27 J at −60 °C, which is not suitable for a long-distance pipeline. In Fig. 8,

Table 6 Impact absorbed energy of outer arc side at different temperatures

Temperatures	Impact absorbed energy Kv_8 (10 × 10 × 55)							
	J				SA %			
	1	2	3	Avg.	1	2	3	Avg.
20 °C	215	216	220	217	90	90	90	90
0 °C	236	222	236	231	95	90	95	93
−10 °C	220	220	227	223	90	90	90	90
−20 °C	160	181	185	175	60	65	65	63
−40 °C	118	64	30	64	33	10	10	10
−60 °C	22	14	45	27	0	0	5	2

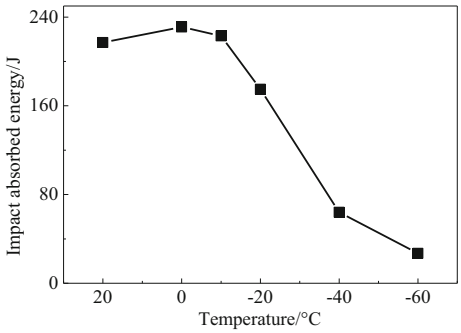

Fig. 7 Ductile-brittle transition curve of outer arc side

the Charpy impact fracture surface at each temperature is shown. The size of dimples increases as the temperature gradually decreases, and the depth decreases with the decrease in temperature. The average shear area at 20, 0, −10 °C are 90, 93 and 90 %, respectively. It can be observed in Fig. 8a–c that the shear area is larger than the others. Until the temperature drops to −40 °C and −60 °C, the fracture changes to brittle fracture characteristics, such as Fig. 8d–f.

The fracture surface of impact toughness tested specimens at outer arc side at different temperatures are shown in Fig. 8. The regions A, B and C are referred to as fibrous, radial and second fibrous area, respectively. The fiber region is expected to absorb higher energy than the radiation section [11]. Compared to −40, −60 °C, the fracture surface at 20, 0, −10 °C, indicates a high proportion of fibrous zone. With the decrease of the test temperature, the fiber area ratio reduces, and the fracture surface appears flat. Impact fracture surfaces under −40 and −60 °C hardly contain fiber area.

At various test temperatures, high magnification SEM fracture toughness tested surface morphology are shown in Fig. 9. There are large and small-sized dimples in region A. Radiation section B shows some features of quasi-cleavage plane, small dimples and tear ridge, the content of these features also reflect the toughness. Zone C representing the second fibrous zone consists of small and large dimples with elongated morphology. As the temperature decreases, the large dimples diminishes gradually, and there are no large dimples at tested temperature of −40 and −60 °C. Only Small dimples are observed both at tested temperature of −40 and −60 °C in A and C. Relatively, large-sized quasi-cleavage facets are observed in B. Large and deep dimples mean superior toughness [22].

Toughness predominantly depends on fraction of the high angle grain boundaries (>15°) and the crack initiators (pearlite, cementite, M/A constituents, and inclusions) [22]. It can be seen in Fig. 4a, b that the microstructure at outer arc side is comprised of high fraction and finer polygonal ferrite. Polygonal ferrite consist of high angle grain boundaries and the effective grain size of polygonal ferrite is smaller and can prevent crack propagation.

4 Discussion

X90 pipeline steel is a kind of low carbon bainitic/ferritic multiphase steels by controlled rolling and cooling, composed of uniform and fine granular bainite and ferrite, with smaller M/A island, which is dispersed distribution (see Fig. 1). Compared with the traditional ferritic steel, X90 steel no longer rely on the incremental C content to increase the strength simply, but mostly rely on three kind of strengthening. On the one hand, controlled rolling results in high density dislocation by deformation in the microstructure, thus inducing the phase transformation strengthening. On the other hand, there is strengthening effect on X90 steel after the phase transition. Fine grains contain the bainitic with a high density of dislocations, dislocation substructure, M/A hardening phase. In addition, precipitation strengthening induced by the micro-alloying elements such as Ti, Nb, V carbonitride also exist [24–26].

Thermo-mechanical controlled processing (TMCP) is the satisfactory method to obtain the strength-toughness

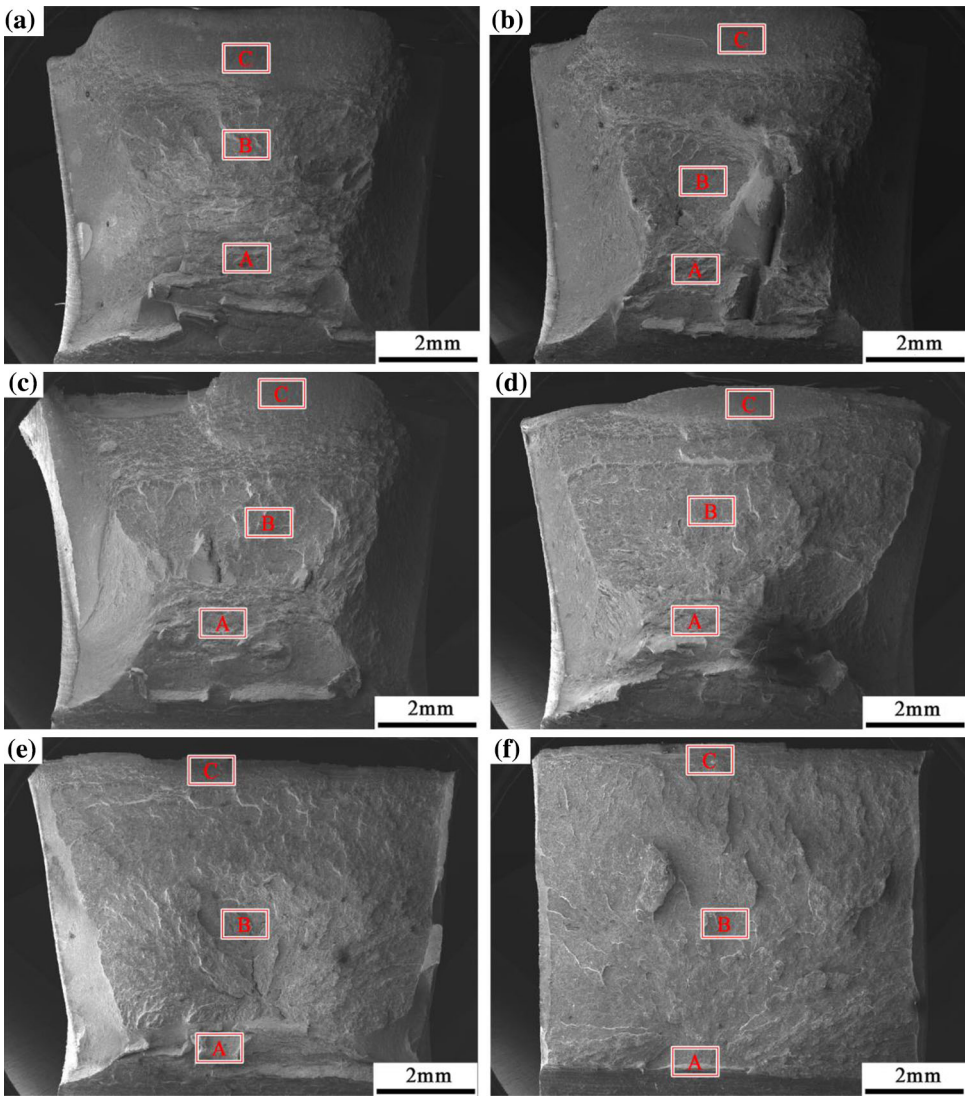

Fig. 8 Fracture surfaces of impact toughness tested specimens at outer arc side for different temperatures **a** 20 °C; **b** 0 °C; **c** −10 °C; **d** −20 °C; **e** −40 °C; **f** −60 °C

combination, which contribute to the increase in strength via microstructural refinement, precipitation hardening and solid solution strengthening as well as strengthening through microstructural modification [27]. Three ways combined with each other, enhances the X90 steel strength greatly. However, by improving the strength, it also relies on multi-phase structure of ferrite to improve the plasticity and to ensure absence of stress concentration effects of bainite, during the plastic deformation process. This increases work hardening capacity, thereby reducing the yield ratio and improving the safety performance. Of course, the high angle grain boundaries of bainite to resist crack propagation is efficient. Due to the fine grain, cracks in the expansion process engage each other, and are obstructed by the fine and intertwined lathes, thus improving the strength and toughness effectively, while the toughness also relies on high density dislocation and sub-structure in ferritic greatly [25]. In addition, the total area of the grain boundaries increases with grain refinement, resulting in increase in the resistance to crack growth, stop crack initiation, both of which work together to reduce ductile–brittle transition temperature.

There is a tendency that during the microstructure transformation from non-equilibrium, that forms after austenitizing and water cooling, to steady state, tempering process provides a thermodynamic conditions for the transformation, and a good strength and toughness bend is obtained. The controlled rolling effect is reduced after local deformation again, because X90 is controlled rolling steel, and the original microstructure also changes, and affect the mechanical properties of steel, especially to reduce the strength. However, for X90 parent pipe with good micro-alloy design, and heating to 1000 °C for deformation, the dissolved micro-alloying elements Nb, V, Ti carbonitrides pin the grain boundaries and dislocations in the form of particle, stop austenite grain growth [25, 26]. When the

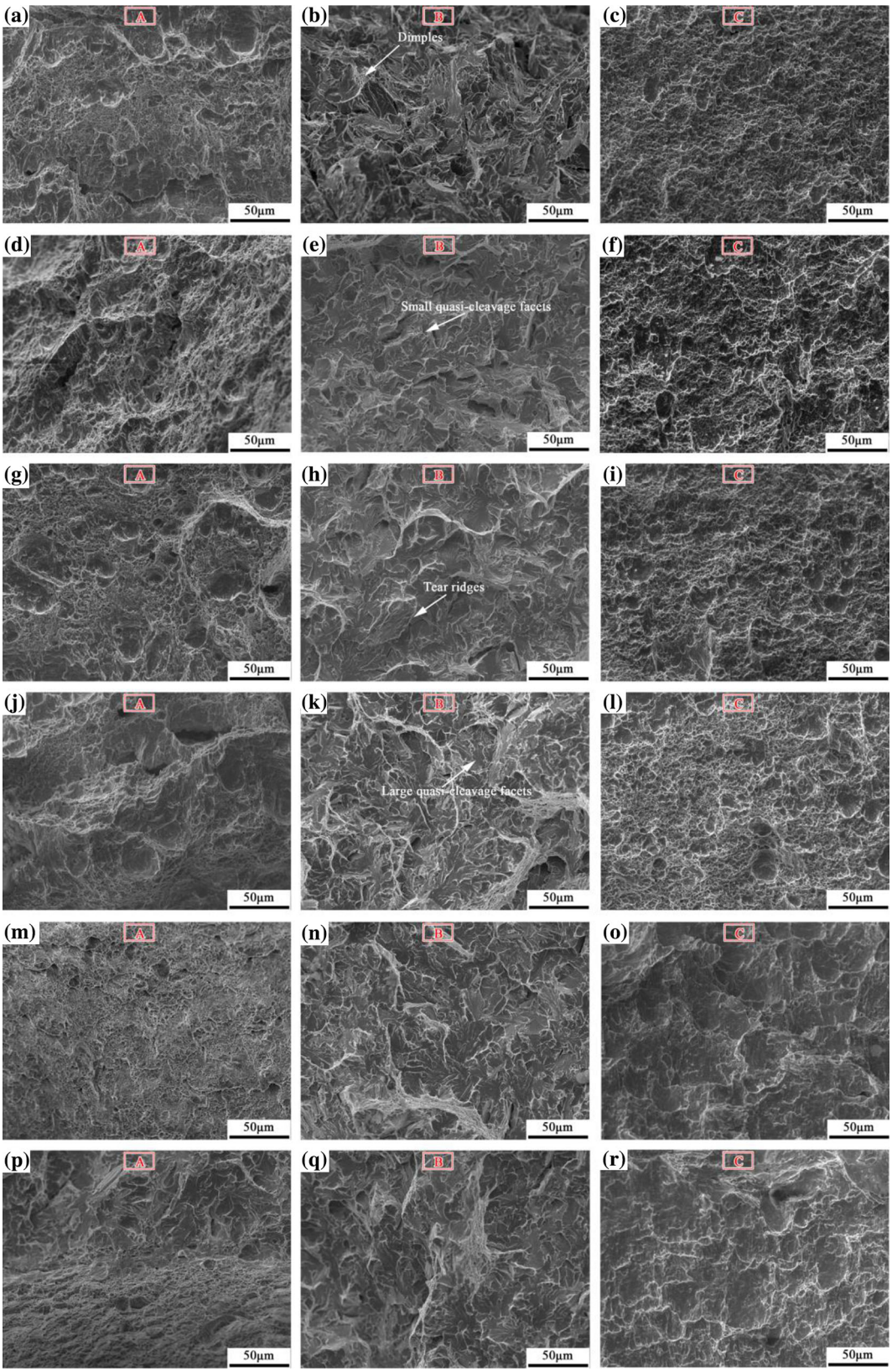

Fig. 9 High magnification SEM fractograghs of impact toughness tested fractures at outer arc side for different test temperatures **a–c** 20 °C; **d–f** 0 °C; **g–i** −10 °C; **j–l** −20 °C; **m–o** −40 °C; **p–r** −60 °C

tempering temperature is 560 °C, a portion of dislocation cancel or disappear, while there is Nb, V, Ti carbonitrides precipitation that strengthens the material. This strengthening mechanism at lower temperature, lay a good microstructure foundation to improve the strength and toughness for X90 local induction bending.

5 Conclusions

By the local induction bending of 1000 °C quenching + 500 °C tempering, microstructure and mechanical behavior of X90 bend have been described as follows:

(1) The microstructure of X90 mother pipe was a composite phase consisting of quasi-polygonal ferrite (QPF), granular bainite (GB) and a small amount of M/A constituents, which was dispersed in matrix in the form of particles and strips. The yield strength, tensile strength, yield ratio was 786, 876 MPa, 0.90, respectively.

(2) There was little difference in the microstructure of X90 bend at different positions, which was related to the force of the bending process. The inner arc side and out arc side of X90 pipe were subjected to pressure and tensile stress, respectively. Polygonal ferrite and lath martensite were formed by dynamic strain induced transformation; the neutral axis was free of force, and the microstructure was the characterization of quenching and tempering, and the grains were small.

(3) After local induction bending, the strength of bend was lower than the parent pipe, but it still showed strong strength. The charpy impact energy was high at a temperature of −10 °C at different positions, which showed good toughness. X90 bend after the process parameters exhibited excellent strength-toughness.

(4) The impact toughness of outer arc side of bend declined in −20 ∼ −40 °C sharply, showing the ductile–brittle transition temperature for the bend within this temperature range; the impact toughness at −60 °C as to 27 J and was not suitable for use as a pipeline.

References

1. API Specification 5L, Specification for line pipe, 45rd (edn), American Petroleum Institute. (2013), p. 32.
2. Zhao W, Wang W, Chen S, and Qu J, Mater Sci Eng A **528** (2011) 7417.
3. Fazackerley W J, Manuel P A, and Christensen L, in Microalloyed steels for the oil and gas industry, TMS 2006.
4. Fukuda N, Yatabe H, and Masuda T, in Proceedings of the 21th International Conference on Offshore and Mechanics and Arctics Engineering, Oslo, Norway, OMAE2002-28210, 2002.
5. Zhong H, J Mater Process Technol **91** (1999) 71.
6. Lee H-W, Bae J-H, and Kim M-S, Int J Precis Eng Manuf **6** (2011) 1051.
7. Xun W, Jie Z, and Qiang L, Procedia Eng **81** (2014) 2255.
8. Zhong H, J Mater Process Technol **102** (2000) 103.
9. Collie G J, and Black I, JMEPEG **20** (2011) 90.
10. ZuTang W, and Zhong H, J Mater Process Technol **21** (1990) 275.
11. Kathayat T, Hill T, Goyal R K, Dhar S, in Offshore Technology Conference (2012).
12. Makovetskii A N, and Mirzaev D A, Phys Met Metallogr **110** (2010) 398.
13. Kondo K, Arai Y, Hirata H, Hamada M, Kitoshio K, Hisamune N, and Murase T, in Proceedings of the Biennial International Pipeline Conference, vol. 3, IPC, (2009) 49.
14. Wang X, Xiao F-r, Fu Y-h, Chena X-w, and Liao B, Mater Sci Eng A **530** (2011) 539.
15. Xu W, Liao B, Wu D Y, Han X, and Zhang Y, J Iron Steel Res Int **12** (2014) 1129.
16. Ahn S T, Kim D S, and Nam W J, J Mater Process Technol 160 (2005) 54.
17. Takahashi N, Shitamoto H, and Fujita S, Proceedings of the Nineteenth International Offshore and Polar Engineering Conference **7** (2009) 21.
18. Zhou T, Yu H, Hu J, and Wang S, Mater Sci Eng A **615** (2014) 436.
19. Annual Book of ASTM Standards, ASTM Designation, E8 and E23, vol. 03.01, Philadelphia, PA, (1995) 142.
20. Beladi H, Kelly GL, and Hodgson PD, Int Mater Rev **55** (2007) 14.
21. Sun L, Muszka K, Wynne B P, and Palmiere E J, Acta Mater **66** (2014) 132.
22. Hu J, Mater Sci Eng A **607** (2014) 122.
23. Hemmerich E, Rolfe B, Hodgson P D, and Weissa M, Mater Sci Eng A **528** (2011) 3302.
24. Hua J, Du L -X, Wang J -J, Xie H, Gao C -R, and Misra R D K, Mater Sci Eng A **587** (2013) 197.
25. Guoa A, Misraa R D K, Xu J, Guo B, and Jansto S G, Mater Sci Eng A **527** (2010) 3886.
26. Bott I S, Vieira A A H, de Souza L F G, and Rios P R, Mater Sci Forum **638** (2010) 3146.
27. Soliman M, and Palkowski H, Mater Des **88** (2015) 759.